buildings

MDPI

Article

Efficiency Assessment on Roof Geometry and Trombe Wall Shape for Improving Buildings' Heating Performance

Maher Dhahri [1,2,3], Ahmet Yüksel [4], Hana Aouinet [3], Di Wang [5,*], Müslüm Arıcı [6,7,*] and Habib Sammouda [2]

[1] Higher Institute of Applied Sciences and Technology of Sousse, Sousse University, Cité Ettafala, Ibn Khaldoun, Sousse BP 4003, Tunisia
[2] Laboratory of Energy and Materials (LabEM) (LR11ES34), High School of Sciences and Technology of Hammam Sousse, Sousse University, Sousse BP 4011, Tunisia
[3] Aeronautics and Aerospace Engineering School, Elisa Aerospace, 48 Rue Raspail, 02100 Saint-Quentin, France
[4] Electric and Energy Department, Yalova Vocational School, Yalova University, Yalova 77200, Turkey; ahmet.yuksel@yalova.edu.tr
[5] School of Physics and Electronic Engineering, Northeast Petroleum University, Daqing 163318, China
[6] Mechanical Engineering Department, Engineering Faculty, Kocaeli University, Kocaeli 41001, Turkey
[7] International Joint Laboratory on Low-Carbon and New-Energy Nexus Research and Development, Kocaeli University, Kocaeli 41001, Turkey
* Correspondence: wangdinepu@stu.nepu.edu.cn (D.W.); muslumarici@gmail.com (M.A.)

Abstract: It is crucial to consider structural design issues in Trombe wall (T-wall) buildings to promote more suitable indoor climates and thermal comfort standards. Therefore, the present study examined the impact of two different T-wall designs and six different roof types on the energy and operational efficiency of a building located in a low-temperature and high-humidity winter climate. Ansys-CFX 15.0 software was employed to simulate the thermal and fluid dynamics behavior of the T-wall system, and flow, thermal comfort, energy, and exergy analyses were conducted. Three-dimensional simulation results and the pertinent literature data showed a good level of agreement, and the accuracy of the model was ensured. Outcomes revealed an average air velocity variation of 0.186 m/s and maximum average indoor air temperature variation of 3.3 °C between the six roof geometries. The highest air speed (0.988 m/s) was recorded for the gambrel roof while the lowest one (0.802 m/s) was recorded for the typical flat roof. The shed roof right with a rounded T-wall was more comfortable for standing and sitting activity than the others for the two T-wall shapes, and, at Y = 0.6 m and Y = 1.1 m, the average predicted percentages of dissatisfied (PPD) values were 31 and 28%, respectively. Furthermore, it was determined in the study that solar radiation intensity and T-wall and roof geometries had a significant effect on energy and exergy efficiency, and high energy and exergy efficiencies were achieved at higher solar intensity values. The best energy and exergy efficiencies were obtained for the butterfly and shed roof configurations. This study can serve as a reference for the thermal environment design of buildings with T-walls.

Keywords: buildings; computational fluid dynamics; heating performance; roof configuration; thermal comfort; Trombe wall

check for updates

Citation: Dhahri, M.; Yüksel, A.; Aouinet, H.; Wang, D.; Arıcı, M.; Sammouda, H. Efficiency Assessment on Roof Geometry and Trombe Wall Shape for Improving Buildings' Heating Performance. *Buildings* **2024**, *14*, 1297. https://doi.org/10.3390/buildings14051297

Academic Editor: Francesco Nocera

Received: 8 March 2024
Revised: 8 April 2024
Accepted: 26 April 2024
Published: 4 May 2024

1. Introduction

Researchers are increasingly showing interest in solar energy applications because of their enormous benefits for sustainable development, including energy conservation, cost reduction, and environmental protection [1,2]. Trombe walls (T-walls), first used in France in 1967, are one of the passive solar energy applications that provide energy savings in the air conditioning of buildings [3,4]. Therefore, various concepts, methods, and experimental systems have been developed, with many studies being conducted on the T-wall by researchers in recent years [5–7].

Most existing photovoltaic (PV) T-wall systems have low efficiency and inadequate for space heating [8,9]. Wang et al. [10] recently proposed a novel microchannel heat pipe–PV T-wall system, in which a heat pipe and a T-wall were used to cool the PV unit to lower the operating temperature and improve the overall efficiency and thermal comfort. Guo et al. [11] conducted a comparative experiment between T-wall buildings and glass façade buildings. Simulations were performed to analyze buildings' indoor thermal climate with different air duct thicknesses. Outcomes revealed that T-wall buildings outperform glass facades and are particularly suitable for regions with high solar intensity and high temperature differences between diurnal and nocturnal periods. Askari and Jahangir [12] proposed the addition of phase-change materials (PCMs) to the T-wall to augment its efficiency. Two layers of PCMs with different phase transition temperatures were used in the building's exterior wall. The results demonstrated the potential of nearly 40% annual energy savings. Baïri et al. [13] experimentally investigated the relationship between the active cavity of a T-wall-type assembly operating in the heating mode and natural convection heat transfer. The authors proposed correlations to calculate the mean Nusselt number of natural convections for a conventional T-wall. The raising of the cavity's aspect ratio from 0.1 to 0.2 resulted in a 13% increase in heat transmission in the active cavity. Ma et al. [14] explored the effect of three different ventilated T-walls on the energy consumption in a room. The heating efficiency and energy savings of a double-ventilated room with and without a T-wall were compared in the study. In the case of using a double-ventilated room with a T-wall, it was determined that the heating efficiency was 32.6% better and that energy savings of 52.6 kWh/m^2 were achieved. Zhang et al. [15] used the simulation technique and field measurements to assess a conventional T-wall in a structure. The study considered four primary impact factors: storage wall material, thickness, glazing angle, and cavity spacing. It was discovered that the proper glazing's inclination angle and wall-to-T-wall ratio were the most crucial elements. The desired residential building's glazing inclination that worked best for the local climate was 10°. Wu et al. [16] suggested a modified form of channel entry and exit to improve T-wall performance. The effects of channel width, height, and different solar irradiation intensities of the T-wall on thermal performance and air purification performance were studied. The results in this paper demonstrated that, for traditional duct entrance and exit methods, the thermal efficacy was less influenced by the duct's height and decreased with increasing width; where solar radiation was larger than 400 W/m^2, the trend downward displayed minor oscillations.

The dynamically coupled water flow channel model of the water-louvered T-wall system was constructed with experimental validation as Hu et al. [17] proposed a novel T-wall using louvers as shade. The absorber plate should be used at higher temperatures to reduce overall exergy destruction and boost exergy efficiency since the exergy destruction associated with its absorption is the highest. The simulated results suggested that the planned T-wall system's monthly mean thermal efficiency varied from 20 to 60% during the heating season and from 30 to 50% during the non-heating season. The thermal performance of two different T-wall types was examined by Duan et al. [18]. Type-I had an absorbent panel adhered to the heat storage wall, and Type-II had an absorbent panel sandwiched between the glass cover and the heat storage wall. The authors assessed exergy efficiencies for various air duct depths, insolation intensities, and glass cover emissivities, and revealed that the largest exergy destruction was due to absorption of the absorber plate. In a study carried out to develop the T-wall [19], direct current (DC) fans were placed in the upper ventilation holes for stable air circulation. The authors noted that the highest heat load savings were achieved when the T-wall occupied approximately 3% of the floor area. Furthermore, optimization factors for the composite T-wall resulted in approximately 52.3% energy savings compared with before optimization. In a study conducted by Singh and O'Brien [20], the potential of a water-immersed T-wall design to be used as a heat storage medium was examined. The rate of energy reaching the colored acrylic sheet-supported T-wall prototype and stored in water was increased from 60.3% to 83.2% as a result of the 5 h experiment. Therefore, it was suggested that the heated water stored in the T-wall could be used as preheating water in buildings during the cold season.

To predict system behaviors and to understand the physics of buildings, the utilization of the computational fluid dynamics (CFD) method is very useful before the construction of buildings in locations where massive urbanization is envisaged [21–23]. Fidaros et al. [24] developed a two-dimensional CFD model to examine 10 different geometric configurations of a T-wall cross-section. In the study, the airflow rate, air mass, velocity distributions, and indoor air temperature of the room were studied. A small gap width of 5 cm was suggested when high air exit temperatures were required. A 5 cm gap width provided a 7 and 11% air temperature increase compared with 7.6 and 10 cm gap widths, respectively. On the other hand, a storage wall with a thickness of 30 cm ensured a 73% increase in the air mass flow rate compared with a thickness of 15 cm. Corasaniti et al. [25] simulated three configurations of a modified T-wall and performed energy and exergy analyses. The comparison between the three configurations demonstrated that the guided flow offered higher thermal efficiency. A two-dimensional numerical model of the thermal performance of the T-wall and air purification were both established in the study by Wu et al. [26]. According to the authors, thermal efficiency was augmented as sun radiation and outside temperature increased. However, the thermal efficiency initially rose and then fell when the channel wideness increased. The maximum thermal efficiency was 52.98% for the level of air purification when the width was 0.04 m.

Some researchers had investigated the effects of roof geometry on the building envelope through energy, economy, and environment analysis [27–29]. In the study by Vaishnani et al. [30], the predicted mean vote (PMV) model was used to evaluate the positions of the openings and the roof slopes, and to determine the comfort zones. The paper's findings showed that the ventilation rate and air distribution pattern were improved at the right roof pitch angles, which had a significant impact on comfort levels. The PMV values decreased as the roof inclination angle was raised, and the ventilation rate of the roof with a 30° inclination angle increased by about 16%. It was also determined that a modest roof pitch was advantageous during the monsoon season. To depict the climatic conditions of the Middle East, Moustafa et al. [31] suggested and thermally tested 14 roof examples between single domes, double domes, and vaults in five distinct arch bases in three different cities (Cairo, Riyadh, and Istanbul). According to the Cairo and Riyadh seasonal conditions, the pointed double dome roof was an effective one, whereas the cases of all roof geometries had convergent results for Istanbul's climatic conditions. Sady et al. [32] explored the influence of various T-wall designs on the energy consumption. The thicker storage wall with a trapezoidal structure and three-sided glass was found to be the optimal design, providing the highest decrease (1637 kWh) in heating load in January, corresponding to 8% higher energy savings compared with those when using a conventional T-wall structure. Using effective roof structure design, Huberman et al. [33] evaluated the energy saving potential of buildings throughout their entire cycle. The study compared the energy demand of reinforced concrete constructions based on traditional flat slabs with those with alternative curved spans using a simulation-based optimization methodology. The results exhibited the potential of non-flat roof structural shapes to reduce energy consumption throughout the life cycle with more than 40% energy savings in the embodied energy and over 25% energy savings accumulated during the life cycle.

Sornek et al. [34] provided a comprehensive review of experimental and numerical studies on different T-wall solutions, including integration with solar chimneys, classic T-walls, T-walls with phase change materials, and photovoltaic T-walls. Shi et al. [35] explored the impact of roof geometry and opening positions on the internal cross-ventilation efficiency of buildings, an aspect crucial for natural ventilation. The research examined three opening configurations (top–top, top–bottom, and bottom–top) and varying slope angles for gable roofs using CFD. The simulations, validated against experimental data, revealed that the highest air exchange efficiency of 48.1% is achieved with the top–bottom opening configuration and a gable roof slope angle of 45°.

Many of the studies analyzed demonstrate that utilizing T-walls for thermal storage contributes to achieving energy efficiency goals, reduces greenhouse gas emissions, and enhances living standards. However, there is a need for more detailed feasibility studies including integration with different roof shapes. There are many works, experiments, and models that have investigated how different aspects of roof design and T-wall configurations influence a building's ability to efficiently capture and utilize solar heat for heating purposes.

By reviewing this research, one can understand optimal roof orientations and angles to maximize solar exposure while minimizing heat loss, as well as effective T-wall designs for absorbing, storing, and distributing solar heat in buildings. Furthermore, this review provides a basis for evaluating and potentially improving current architectural design practices aimed at improving the thermal performance and energy efficiency of buildings. Previous research has primarily focused on understanding the thermal performance of buildings with different roof geometries without an integrated T-wall and others have studied the performance of the T-wall without integrating different roof shapes consistently. However, most of these studies have concentrated on quantitatively assessing and examining only a flat roof shape for heating or cooling alone, without combining it with other shapes of roof geometry. To promote natural ventilation, retain heat, and make T-wall structures more suitable for indoor climates, thermal comfort standards, and occupant circumstances, it is crucial to take structural design considerations into account. The aim of this research, from a scientific point of view, is to study the effectiveness of Trombe walls in the use of solar energy for residential heating, especially during winter seasons, through a comprehensive analysis of heat transfer and air flow dynamics as well as an analysis of thermal comfort. Additionally, the study aims to validate numerical models to optimize the design parameters of T-walls for improved thermal comfort inside the building that complies with ASHRAE standards. From the perspective of practical technologies for building design and installation, this research aims to provide valuable insights into the design and implementation of T-wall and roof forms as an alternative energy solution for heating buildings. By examining various geometric parameters and using computational fluid dynamics simulations, the study aims to provide practical recommendations for optimizing the design of T-walls to improve thermal comfort in residential spaces. These results can potentially inform architects, engineers, and builders in the effective integration of T-walls into building design, thereby contributing to more sustainable and energy-efficient construction practices.

2. Materials and Method

In this study, the effects of six roof configurations and two T-wall geometries on flow, thermal comfort, energy, and exergy efficiency were evaluated via CFD analysis. Simulations were performed under the weather conditions of Sousse, Tunisia, in January. The city of Sousse (35°49′34″ N and 10°38′24″ E) is located 143 km south of Tunisia and at an altitude of 25 m. The urban climate is characterized by continuous solar radiation that is strong in sunlight and solitude throughout the year. In the summer, the relative humidity is around 67% and the air temperature under the shade is around 43 °C. In addition, during the daytime in winter, the outside air temperature of ten ranges between 10 °C and 20 °C, and in the event of insufficient or irregular rain, it might fall to less than 1 °C at night. For other required values, sample values given in studies in the literature were used [36–39].

2.1. Mathematical Model, Geometric Configurations, and CFD Setup

The continuity, energy, and momentum equations used in the simulation analyses are each given below [36]:

$$\frac{\partial \rho}{\partial t} + \frac{\partial}{\partial x_I}(\rho u_j) = 0 \tag{1}$$

$$\rho\frac{\partial u}{\partial t} + \rho(u.\nabla)u = \nabla\left[-pl + (\mu+\mu_T)\left(\nabla u + (\nabla u)^T\right) - \frac{2}{3}\left((\mu+\mu_T)(\nabla.u)l - \frac{2}{3}\rho kl\right)\right] + F \tag{2}$$

$$\frac{\partial \rho}{\partial t}(\rho C_a T) + \frac{\partial}{\partial x_j}(\rho u_j C_a T) - \frac{\partial}{\partial x_j}\left(\lambda \frac{\partial T}{\partial x_j}\right) = s_T \tag{3}$$

The equations for the turbulence kinetic energy (k) and dissipation rate (ε) are as follows [37]:

$$\frac{\partial}{\partial t}(\rho k) + \frac{\partial}{\partial I}(\rho k U_i) I \frac{\partial}{\partial x_j}\left[\left(\mu + \frac{\mu_t}{\sigma_k}\right)\frac{\partial k}{\partial x_j}\right] + G_k + G_b - \rho\varepsilon - Y_M + S_k \tag{4}$$

$$\frac{\partial}{\partial t}(\rho \varepsilon) + \frac{\partial}{\partial x_i} I = \frac{\partial}{\partial x_I}\left[\left(\mu + \frac{\mu_t}{\sigma_\varepsilon}\right)\frac{\partial \varepsilon}{\partial x_j}\right] + C_{1\varepsilon}\frac{\varepsilon}{k}(G_k + C_{3\varepsilon} G_b) - C_{2\varepsilon}\rho\frac{\varepsilon^2}{k} + S_\varepsilon \tag{5}$$

The turbulent viscosity (v_t) is calculated as follows:

$$v_t = C_\mu \frac{k^2}{\varepsilon} \tag{6}$$

The flow is classified as laminar if the Rayleigh (Ra) value is less than 10^8 and turbulent if the Ra value is larger than 10^9. The transitional region lies between Ra values of 10^8 and 10^9. Ra is given as follows:

$$Ra = \frac{g \cdot \beta \cdot \Delta T \cdot L^3}{\nu \cdot \alpha} \tag{7}$$

In this study, ANSYS-CFX (15.0) software, a commercial CFD tool, was employed to simulate the thermal and fluid dynamic behavior of the T-wall system. This software utilizes the finite volume discretization approach to solve the governing equations in the computational domain [38,39]. Figures 1 and 2 display the six configurations of roof geometry and the two configurations of T-wall geometry. One of the T-walls was a flat wall, and the other was a wall with rounded corners. Roof geometries were considered to be conventional (A and G), gable (B and H), butterfly (C and I), gambrel (D and J), or shed (E, F, K, and L) roofs.

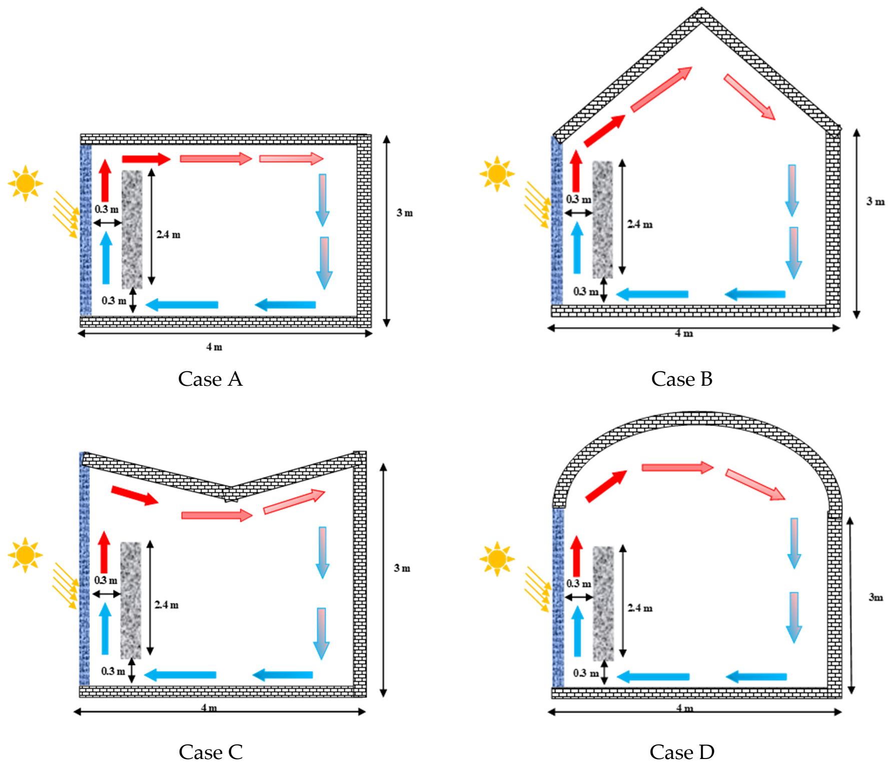

Figure 1. *Cont.*

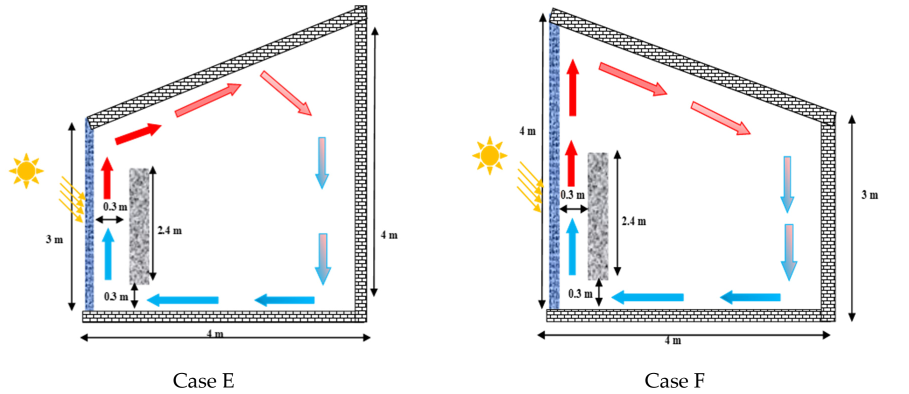

Figure 1. Configurations of roof and flat T-wall.

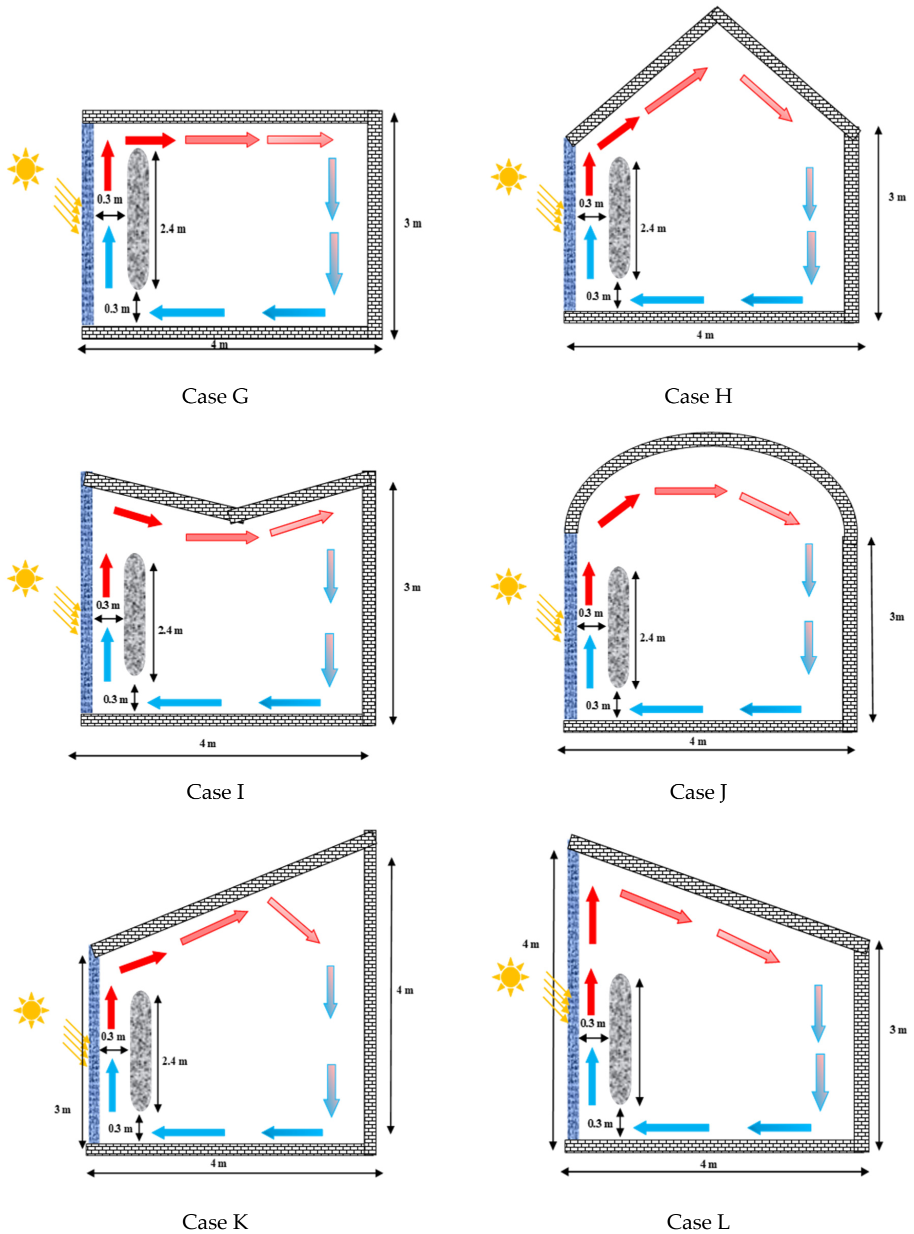

Figure 2. Configurations of roof and rounded T-wall.

Previous studies [40–42] have demonstrated that T-walls with a flat wall and others with rounded corners always improve thermal efficiency and the total efficiency. For this reason, these two different T-wall designs (flat and rounded), and Gable, butterfly, candelabra, and shed roof designs were chosen to be examined in this article due to their important functions. In the study, it is considered that the T-wall was located on the south side of a simple room. The room had height × length × width dimensions of 3 × 4 × 4 m^3. Furthermore, the thickness of T-wall and air gap was 0.3 m, and the height of the T-wall was 2.4 m. This solar system received the maximum energy when oriented towards the south and was inclined at an angle almost equal to the latitude of the place (Sousse).

2.2. Boundary Conditions and Mesh Independence

Table 1 summarizes the specified boundary conditions. Several studies conducted earlier by different authors provide support for the building of the T-wall under consideration, particularly with regard to the thickness of the air layer [36,43,44].

Table 1. Boundary conditions.

Element	Temperature (°C)	Wall Type	Heat Transfer Coefficient (W/m^2K)
Roof	45	Non-transparent	250
Front wall	45	Non-transparent	250
Floor	30	Non-transparent	-
Glazing	45	Transparent	-
T-wall	-	Non-transparent	800
Other walls	Insulated	Non-transparent	-

In this study, a structured mesh based on a rectangular grid was used, and grid independence was tested utilizing four cases of meshes with mesh numbers of 62,908, 112,356, 132,804, and 164,388 (Figure 3). Simulations were applied on a structured, refined mesh in the channel, contiguous to the wall.

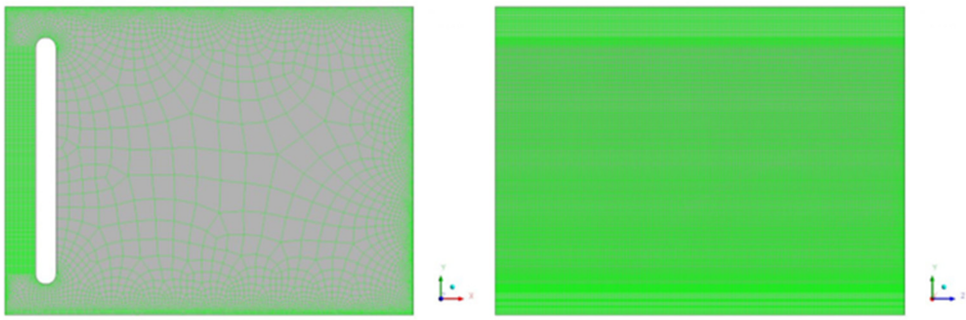

Figure 3. Mesh structure used for CFD.

The grid independence study was performed to validate the numerical stability of the simulation. In this case, the initial heat transfer coefficient in the wall and the T-wall were 250 and 800 W/m^2K. Four structured meshes were adopted with the refined meshes in and near the wall region. The numerical results for these four meshes are shown in Figure 4. From the figure, it is clearly seen that mesh #3 (i.e., the one with 132,804 mesh number) was sufficiently precise for the present model. Increasing the number of cells beyond mesh #3 (i.e., the one with 132,804 mesh number) did not have a significant impact on the results. Moreover, increasing the number of cells prolonged the analysis time. Therefore, mesh #3 was considered in all the computations.

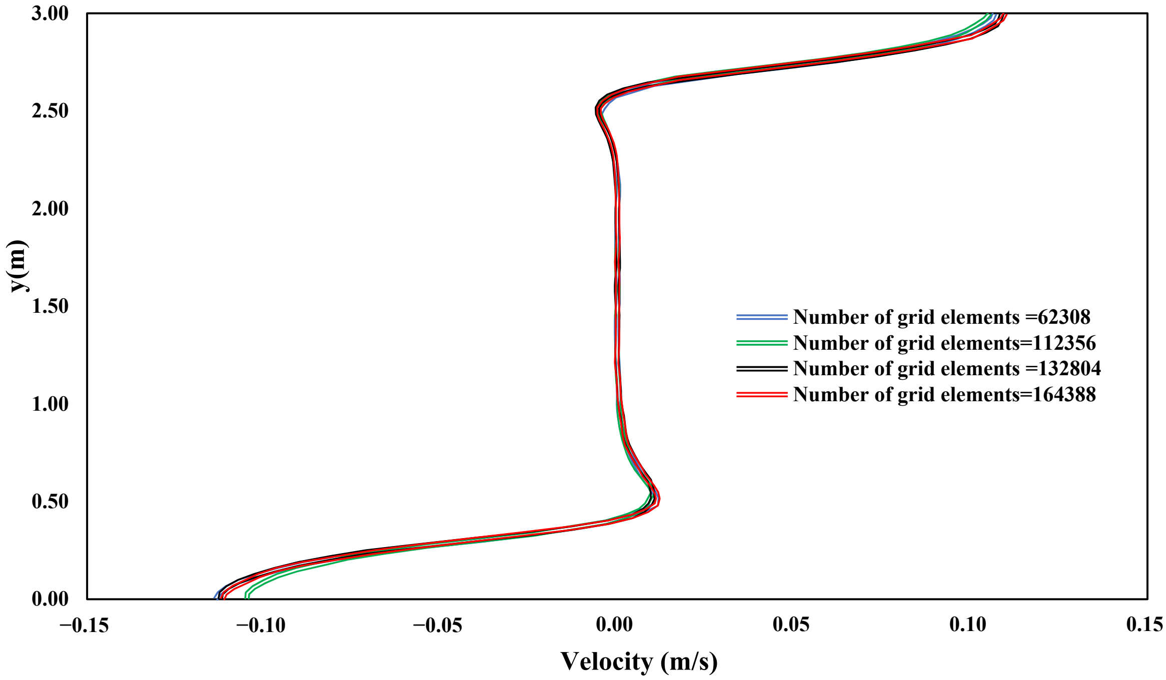

Figure 4. Mesh independence test.

2.3. Energy and Exergy Model

Energy and exergy analyses were carried out to assess the T-wall's thermal performance. Equation (8) can be used to determine the convective heat exchanged in the air duct [18]:

$$q = \dot{m}c_f\left(T_{fo} - T_{fi}\right) \tag{8}$$

The thermal efficiency of each configuration is determined as follows:

$$\eta = \frac{\dot{m}C_p(T_{outlet} - T_{inlet})}{A_p I_{rad}} \tag{9}$$

where A_p is the area of the absorber wall. Furthermore, the exergy balance equation is expressed as follows [18]:

$$\dot{E}_{Xrad} + \sum \dot{E}_{Xin.f} - \sum \dot{E}_{Xout.f} - \sum \dot{E}_{Xloss} - \sum \dot{E}_{Xd} = 0 \tag{10}$$

where $\dot{E}_{Xd}$ is the exergy of solar radiation.

$$\dot{E}_{Xrad} = A_g I_{rad}.\left[1 - \frac{4}{3}.\frac{T_a}{T_s} + \frac{1}{3}.\left(1 - \frac{T_a}{T_s}\right)\right] \tag{11}$$

Here, A_g is the area of glazing. $\dot{E}_{Xin.f}$, $\dot{E}_{Xout.f}$, $\dot{E}_{Xloss}$ and $\dot{E}_{Xd}$ are the exergies of inlet fluid, outlet fluid, lost exergy, and total destroyed exergy due to irreversibility, respectively. $\dot{E}_{Xgain}$ is calculated via the exergy balance in the control volume [18]:

$$\dot{E}_{Xgain} = \dot{E}_{Xout.f} - \dot{E}_{Xin.f} = \dot{m}C_p\left(T_{out} - T_{in} - T_a ln\frac{T_{out}}{T_{in}}\right) - \frac{\dot{m}}{\rho}\Delta p\frac{T_a}{T_m} \tag{12}$$

where T_a and T_s are the ambient and sun temperature. The exergy efficiency is described by the ratio between the extracted exergy and the solar radiation exergy (Equation (13)):

$$\eta_{ex} = \frac{\dot{E}_{xgain}}{\dot{E}_{xrad}} \tag{13}$$

2.4. Thermal Comfort Model (PMV-PPD)

To investigate thermal comfort, we employed Fanger's thermal comfort methodology outlined in ASHRAE Standard 55:2017 [45], which was then integrated into the computational fluid dynamics (CFD) simulations for the analyzed scenarios. This approach allows for the estimation of both the percentage of dissatisfied individuals (PPD) and the predicted mean vote (PMV), considering factors such as ambient temperature resulting from convective and radiant heating, relative humidity, air velocity, metabolic rate, and clothing [46,47].

The region where the PPD was below 10% and the PMV is between −0.5 and 0.5 indicated that the environment was acceptable in terms of thermal comfort (Figure 5). The discomfort level of the environment increased as it moved away from these limit values. In the acceptable ranges of PPD and PMV, three types of comfort zones are given in Table 2 [48,49].

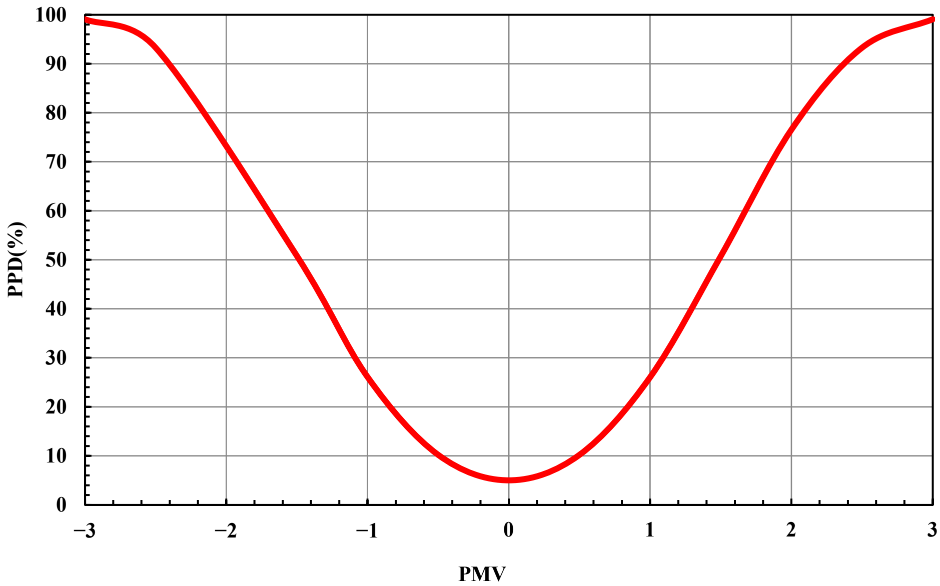

Figure 5. Relationship between PMV and PPD [48,49].

Table 2. PMV-based PPD [49].

Comfort Zone	PPD	PMV
1	<6	−0.2 < PMV < 0.2
2	<10	−0.5 < PMV < 0.5
3	<15	−0.7 < PMV < 0.7

3. Results and Discussion

The roof configurations were analyzed in terms of flow field, thermal comfort, and energy and exergy performance, each of which is discussed below in a subsection.

3.1. Validation of Modeling

The numerical results from CFD were compared with the experimental findings from the study by Duan et al. [18] published in the literature to validate the mathematical model.

Under identical circumstances, a traditional T-wall was used in both tests. Figure 6 displays a comparison of the T-walls' energy efficacy for various insolation intensities. The results were evaluated using the relative error (*RE*) as follows:

$$RE = \left| \frac{X_{exp} - X_{CFD}}{X_{exp}} \right| \times 100 \quad (14)$$

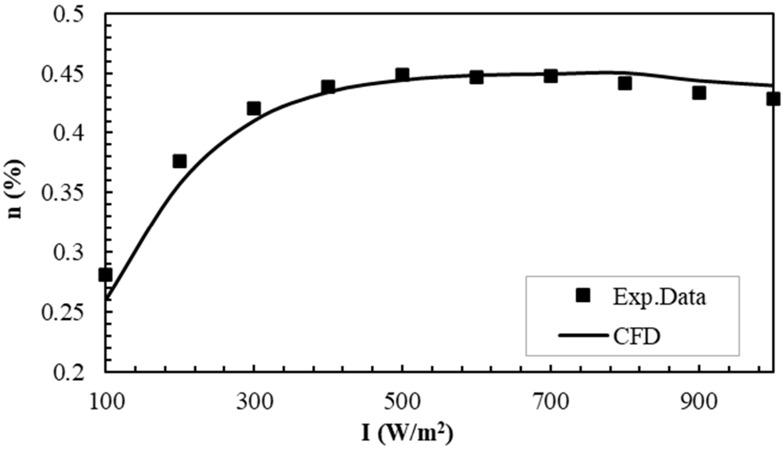

Figure 6. Validation of the mathematical model.

The model's output and the results that have been published show a good degree of agreement. The maximum relative error was 7.29%.

3.2. Flow Analyses

Figures 7 and 8 show the distribution of velocity fields at the Z = 2 m location of the room and the T-wall combinations considered. The heated air in the collector moved towards the air gap with the effect of buoyancy. The results confirm that the geometry of the roof and T-wall have a direct significant effect on the velocity fields inside the building.

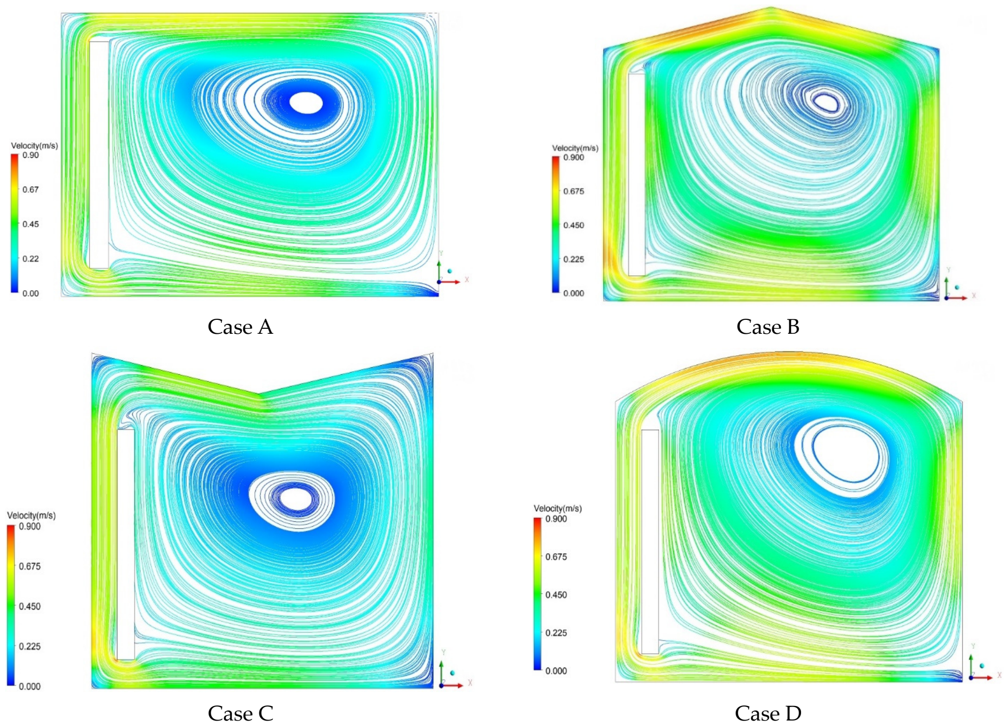

Figure 7. *Cont.*

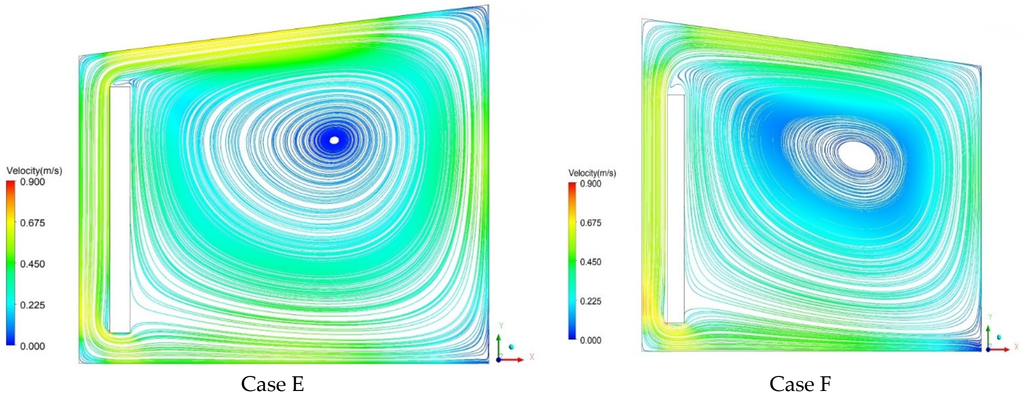

Figure 7. Velocity streamlines for roof configurations and flat T-wall.

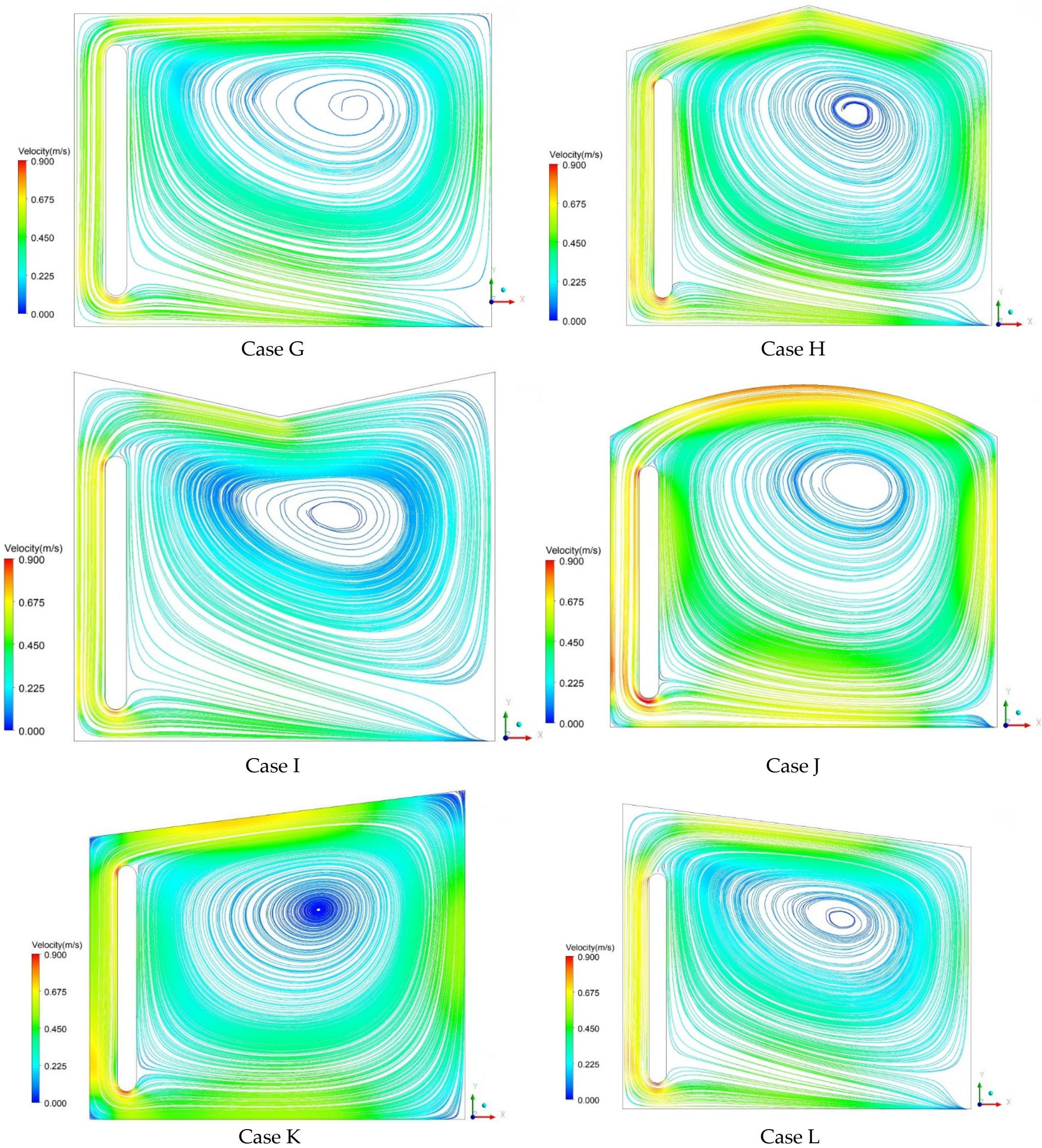

Figure 8. Velocity streamlines for roof configurations and rounded T-wall.

Velocity vector maps clearly demonstrate the locations of recirculation zones as well as high and low velocities. Initially, in every case examined, the solar energy passes through the glass cover and is then absorbed by the T-wall. Hence, some of this energy is transferred to the wall through conduction and the remainder is transferred to the air in the channel by convection. Air is displaced from the bottom of the channel to the top under the influence of the chimney, and this result is in line with previous studies [43]. On the other hand, large recirculation inside the room is observed covering and ventilating the biggest part of the room. It is observed that the air reaching the right wall loses its energy toward the outside of this same wall. As a result, the air is transferred to the lower part of the room and then moves to the bottom of the channel where it was previously further heated by the absorbent wall. This finding is in a good agreement with the flow predicted by Fidaros et al. [24]. A temperature gradient is formed between the locations as a result of this air movement. Furthermore, a tiny vortex is seen to form right at the corner. Near the gap exit, reverse flow patterns are prominent. The airflow is found to have significant turbulence close to the ground and roof. Moreover, flow separation is seen in the channel's corner between the entrance and the air gap. Then, the air flows to the glass under the influence of inertia. The highest velocity is observed in the middle of the elevation since the flow speed increases as there is heat transfer from the air to the central part of the room, which tends to reduce the differences in velocity and temperature across the duct. The maximum air velocities for roof and T-wall configurations are given in Table 3 according to the results obtained from the velocity contours. It was determined that there was not much of a difference between the maximum air velocities of configurations. Air velocities in Cases D and F were comparatively higher than in Cases A, B, C, and E. Moreover, the region affected by the reverse flow for Cases C and F was relatively smaller than that for the other cases. The maximum velocities generated in the building equipped with a rounded T-wall were higher compared with those of the flat T-wall, as well as in the middle region of the domain where the mean air velocity did not exceed 0.25 m/s for all cases. From these results, it can be seen that, for the various cases considered, the location of the maximum and the minimum values of the magnitude velocity are the same for the different considered cases, and the air velocity of the T-wall increases as the temperature difference between the heat storage wall and the glass wall increases. The wind speed is relatively high when the intensity of solar radiation is strong, such as in summer. On the contrary, the wind speed is relatively slow in winter due to weak sun intensity. Therefore, the T-wall could be used to ventilate buildings with relatively high air flow, and it could be used for building heating in winter through relatively slow airflow heated by sunlight.

Table 3. The maximum velocities for the considered roof and T-wall configurations.

Geometry Roof	Velocity (m/s)	
	Plat T-Wall	**Rounded T-Wall**
Classic flat roof (A and G)	0.800	0.813
Gable roof (B and H)	0.819	0.861
Butterfly roof (C and I)	0.826	0.863
Gambrel roof (D and J)	0.841	0.989
Left shed roof (E and K)	0.744	0.891
Right shed roof (F and L)	0.842	0.899

The distributions of the air temperature in the room in the section located at Z = 2 m are shown in Figures 9 and 10 for the different roof and T-wall geometries. Typically, the temperature of the air changed vertically from floor to ceiling, and it was lower on than floor than on the ceiling. The minimum temperature was located at the top right corners of the room for all cases. Furthermore, the high temperatures near the wall were noticeable. The maximum indoor air temperature in the case of a flat T-wall was higher than that in the case of a rounded T-wall (Table 4). Significant changes in temperature across the components of the T-wall were the transmission of solar energy since temperature changes were the fundamental driving force for the T-wall mechanism. These results indicated that the temperature distribution was similar for the different configurations of the airgap considered. For all situations, the determined average temperature for the room's center was 39.4 °C. Because of the difference in density, cold air spreads out at the ground level. The average indoor air temperature dropped by 6.1 °C as a result of this chilly airflow. Since the air temperature difference between a horizontal plane at Y = 0.2 m and the ground was 7 °C in this instance, a phenomenon of overheating in the room was noticed.

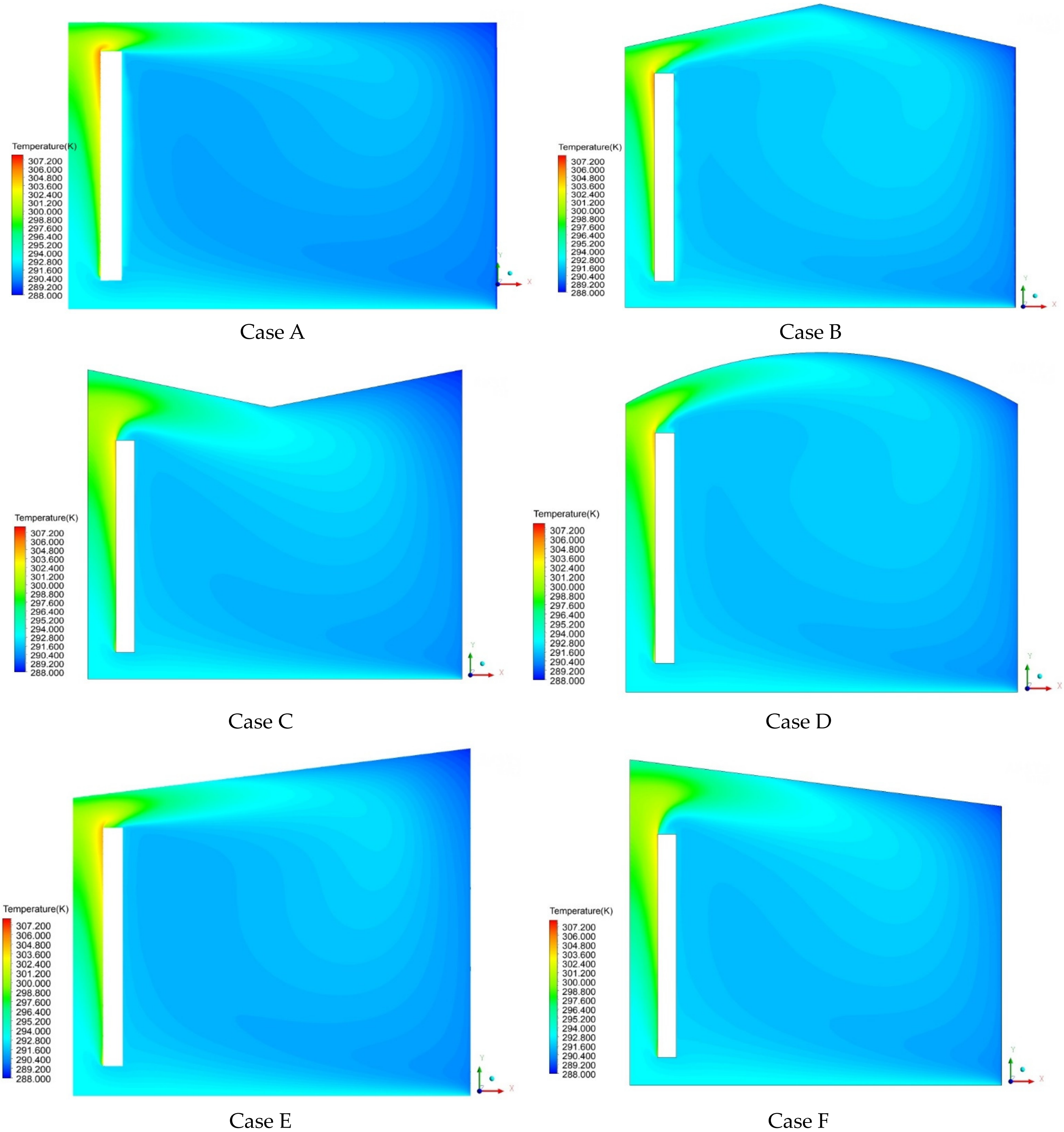

Figure 9. Contours of the indoor air temperature for the roof configurations with flat T-wall.

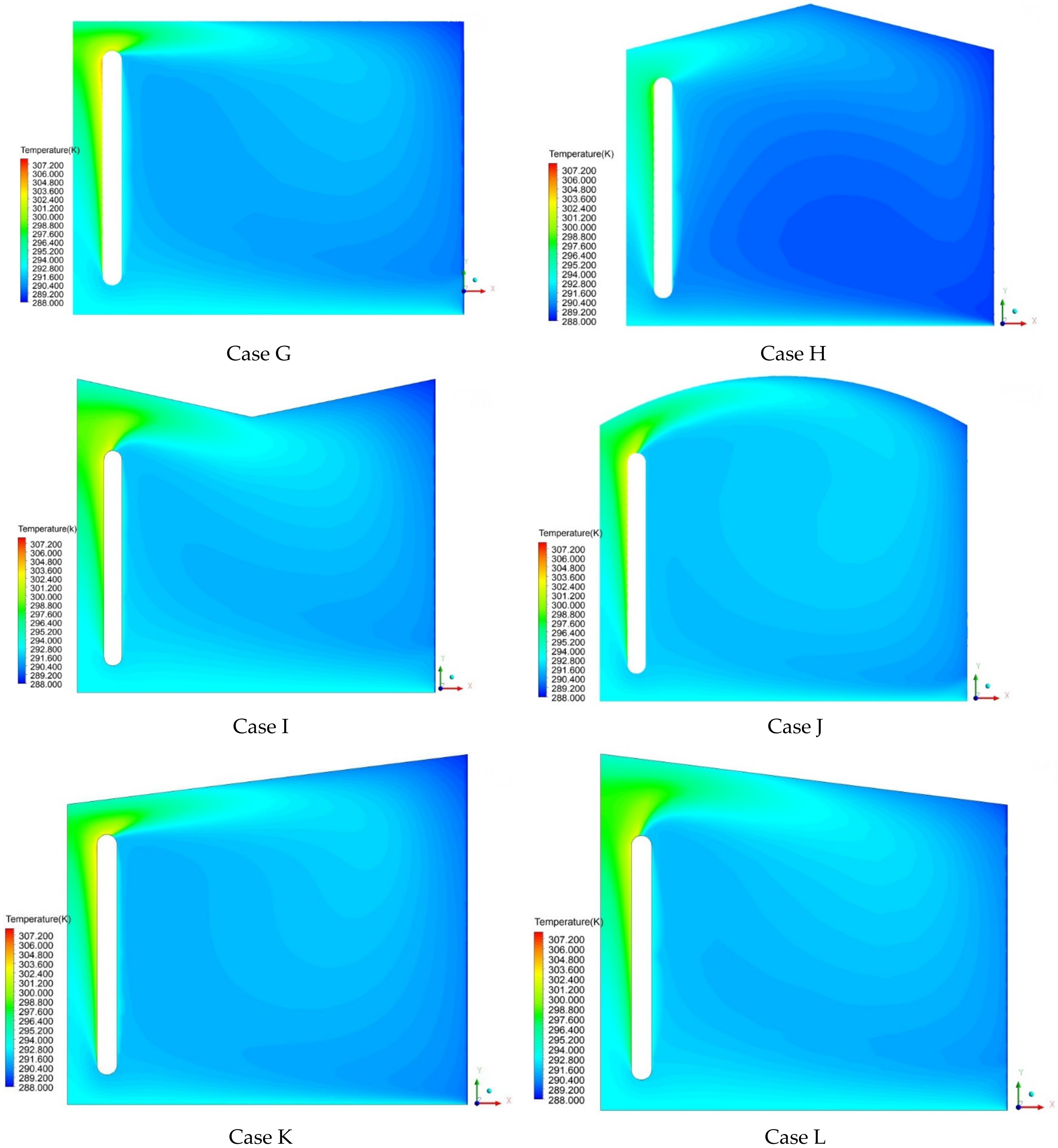

Case G, Case H, Case I, Case J, Case K, Case L

Figure 10. Contours of the indoor air temperature for the roof configurations with a rounded T-wall.

Table 4. The maximum temperature for roof and T-wall configurations.

Geometry Roof	Temperature (K)	
	Plat T-Wall	Rounded T-Wall
Classic flat roof (A and G)	306.3	304.6
Gable roof (B and H)	305.1	303.8
Butterfly roof (C and I)	304.6	303.4
Gambrel roof (D and J),	304.9	303.76
Left shed roof (E and K)	305.2	304.2
Right shed roof (F and L)	304.3	303.03

3.3. Thermal Comfort Analysis

Investigating the effects of roof geometry and T-wall shape on occupant thermal comfort could provide valuable information to the planner for accomplishing more energy-efficient designs and heat buildings. To map indoor thermal comfort, several influencing parameters must be predicted, including air velocity, temperature, and PMV-PPD indexes. According to ASHRAE Standard 55:2017 [45], when the vertical air temperature difference between 1.7 and 1.0 m above the floor exceeds 3 °C, it is a significant contributor to increased thermal dissatisfaction. In this section, using the Fanger comfort model, the PMV and PPD results of the analysis were interpreted and analyzed at three occupant locations, at the ankles (Y = 0.1 m), torso (Y = 0.6 m), and head (Y = 1.1 m). These three levels are commonly used to assess thermal comfort in buildings and provide useful information for effective building design. In this study, the numerical results of all cases were presented and compared in terms of PMV and PPD.

The PMV distribution contours of the six cases (A, B, C, D, E, and F) of the room equipped with a flat T-wall at the height Y = 0.1 m, Y = 0.6 m, and Y = 1.1 m are shown in Figure 11. The figure indicates that the PMV values of the simulation room for all cases were mainly concentrated from -3 to 3. Similar distributions were observed in the study by Irshad et al. [50], where they stated that the PMV was between 0 and 1 and the PPV was around 15% for the building equipped with a T-wall. The authors determined that these thermal comfort index values were within the range of the recommended ASHRAE Standard 55:2017 [45]. Better thermal comfort was obtained at the Y = 1.1 m level compared with the other two levels where the PMV ranged between 0.5 and 1.5. There was a decrease in thermal comfort inside the room at Y = 0.1 m. At this level, the PMV value was between -2 and -1. This was caused by the low temperature occurring due to natural convection in the region close to the ground. The PMV contours demonstrated nearly similar comfort conditions for the six cases at plane Y = 1.1 m. A cool thermal sensation region (PMV = -3 to -0.5) was found at the Y = 0.1 m level. The cold region was more pronounced for Cases C and F.

The results in Figure 12 demonstrate that the PPD could vary from 5 to 97% depending on the calculated PMV. These comfort values depended on where the resident was located in the building. The PPD should not exceed 20% at each of the occupied points in the room to reach comfort conditions. The PPD contours were almost identical for the six cases at the Y = 1.1 m plane. In this level, the PPD value was between 10 and 45%. Some cold thermal areas disappeared near the T-wall for Cases C and F.

The maximum and minimum average PPD values were, respectively, 61.34 (Case C) and 41.91 (Case D) for Y = 0.1 m (Figure 13). Similar results and observations were found by the authors of [43], in which the optimal design included a 1.7 m height, 0.3 m wall thickness, and 0.22 m channel depth. In the study [43], it was suggested that throughout the entirety of winter, the suggested T-wall maintained thermal comfort levels at 43.88%, significantly surpassing the 9.4% figure indicated by the psychometric chart established according to ASHRAE Standards. For Y = 0.6 m, Case C had an average PPD value of 31.21 and this case was identified as the most comfortable case in comparison with other cases. Furthermore, Case C had an average PMV of -0.39 and an average PPD value of 27.55% for Y = 1.1 m. Thus, a flat T-wall and a butterfly roof can be preferable for good thermal performance.

Figure 14 shows the PMV contours on the vertical profiles (Y = 0.1 m, Y = 0.6 m, and Y = 1.1 m) for the six cases of the room equipped with a rounded T-wall. At first glance, it is clearly seen that PMV values are negative and positive in six cases and at three levels, as the geometric form of the T-wall and roof formed a warm environment in some places and a cool environment in others. Moreover, the PMV values on the upper level of the room are larger than those on the lower area due to the rising of warm air via natural convection. The PMV values in the center of the plane approach zero, and the degree of thermal comfort increases as the height elevates. The PMV values near the wall region are the largest due to this being the region of the heat source.

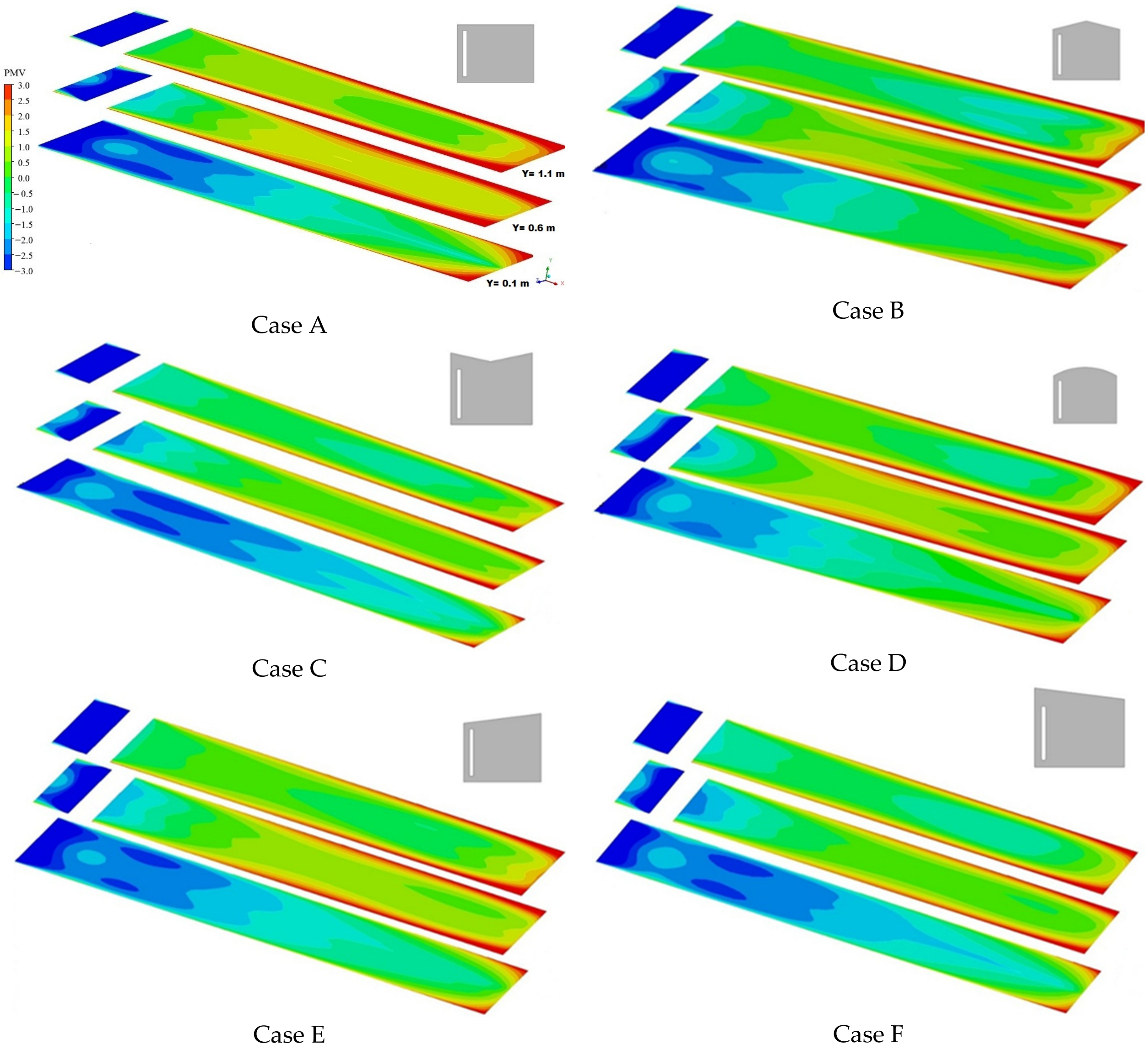

Figure 11. PMV contour for the flat T-wall.

Figure 15 shows the PPD contours for the six cases of the room equipped with a rounded T-wall. The highest degree of thermal satisfaction was registered for all the cases for Y = 1.1 m. Furthermore, at Y = 0.6 m, higher thermal satisfaction was obtained in Cases H, I, and L, compared with the others. For Y = 0.1 m, the PPD was spread over a wide area and was mostly higher than 60%. This situation revealed that this plan did not meet the thermal comfort conditions, and that Case L had the best thermal satisfaction value. The results indicated that the thermal comfort levels at Y = 0.6 m and Y = 1.1 m were acceptable for the six cases studied.

Significant differences in thermal comfort indices were observed for the considered cases at different altitudes (Figure 16). At the Y = 0.1 m level, the PPD values were 52.25, 46.12, 68.41, 39.73, 44.03, and 55.18% for G, H, I, J, K, and L, respectively. A dissimilar trend was observed: 50.31, 33.80, 34.39, 36.29, 36.04, and 33.87% were the average PPD values of the six cases, G, H, I, J, K, and L, for the Y = 0.6 m level, respectively. These values were lower than those among the data at the Y = 0.6 m level. Finally, at the Y = 1.1 m level, the average PPD in case G, H, I, J, K, and L were 37.24, 29.59, 28.51, 36.38, 29.98, and 28.10%. It was determined that Case L was more comfortable than the other conditions at higher levels from the ground.

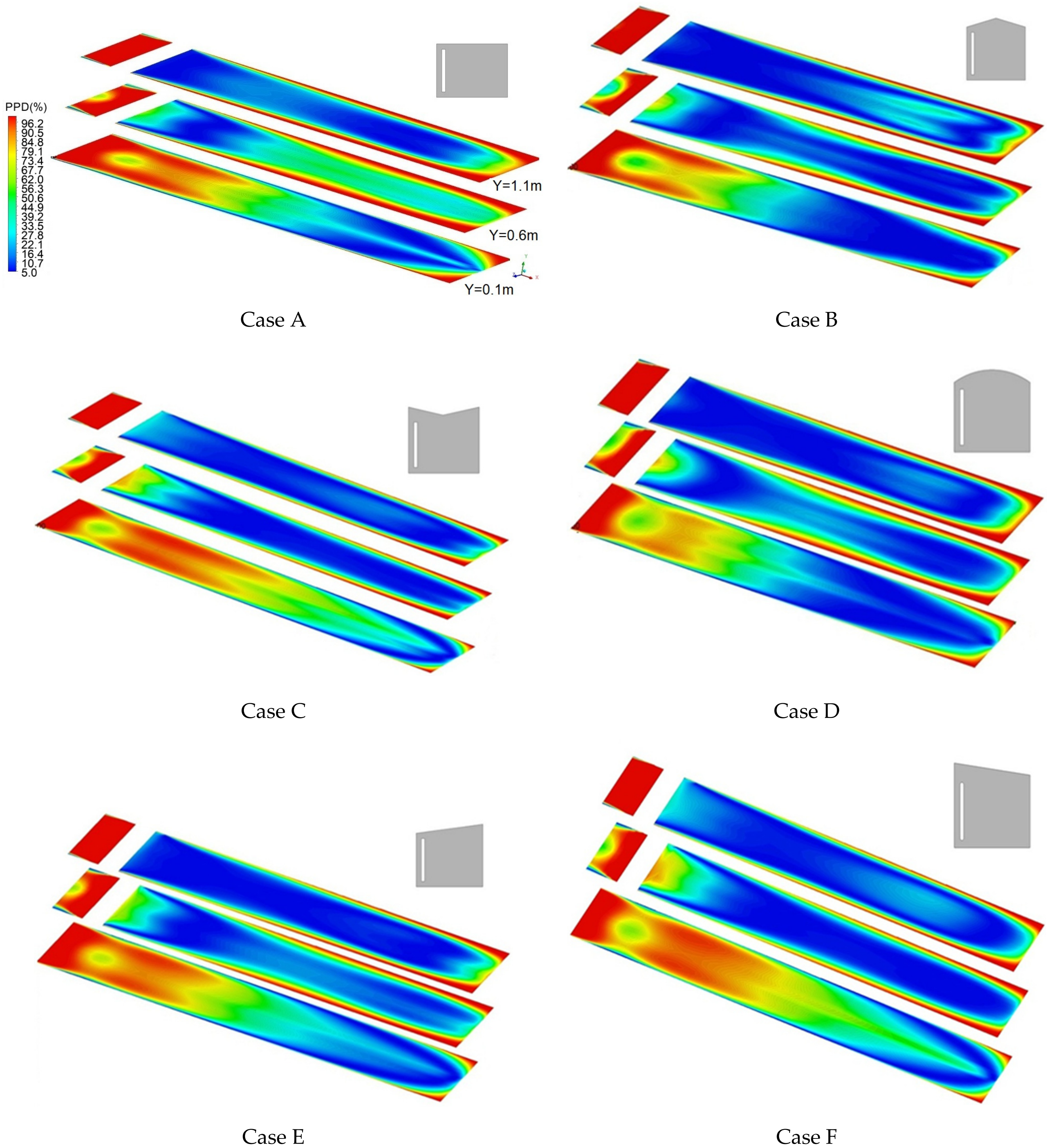

Figure 12. PPD contours for the flat T-wall.

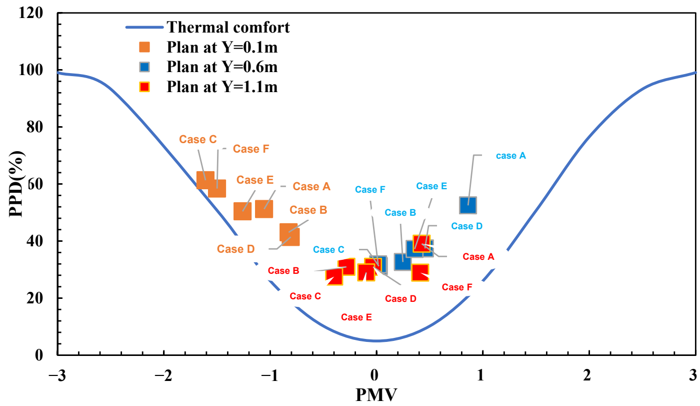

Figure 13. PMV and PPD distributions for six configurations with a flat T-wall.

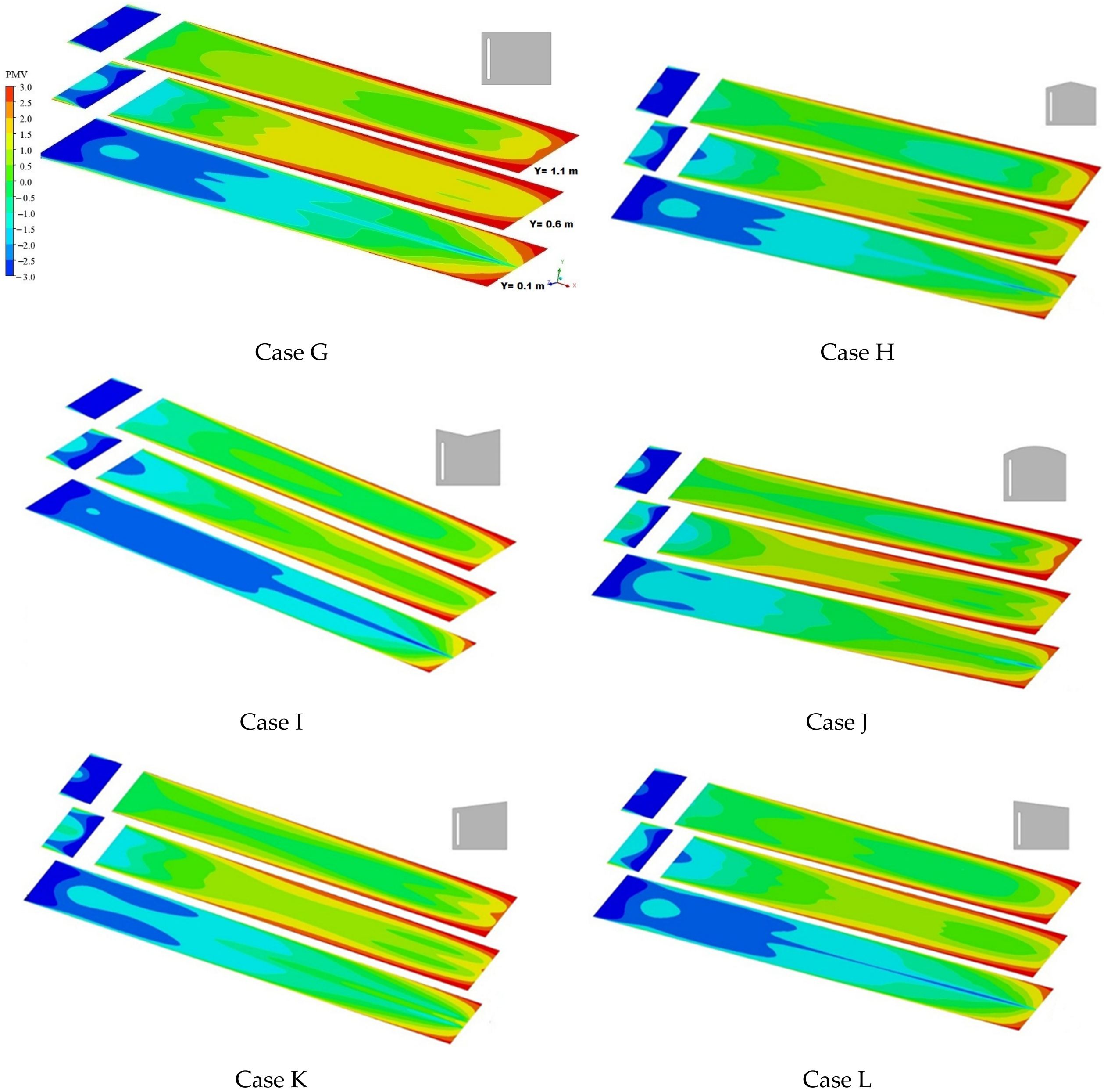

Case G Case H

Case I Case J

Case K Case L

Figure 14. PMV contours for the rounded T-wall.

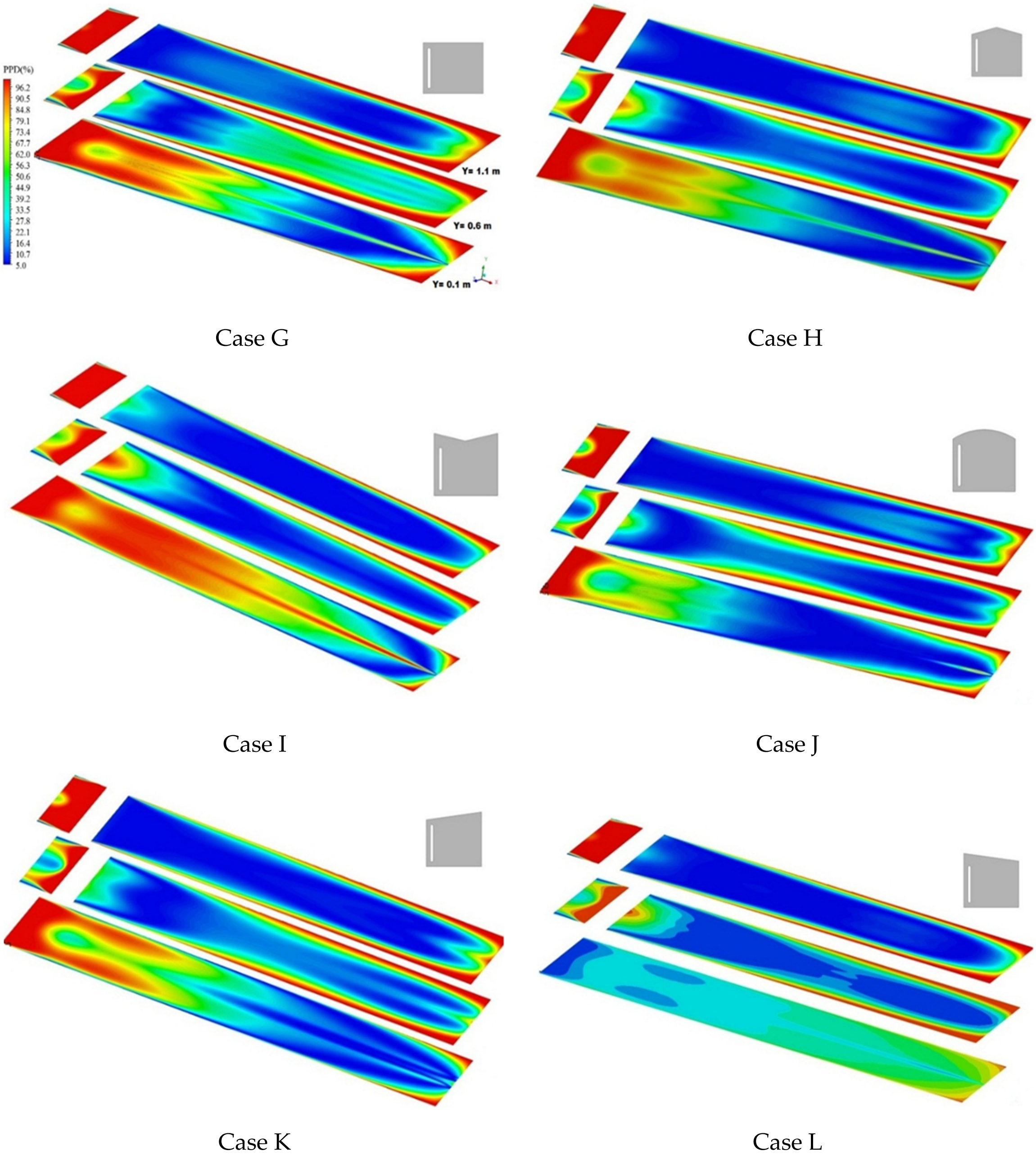

Figure 15. PPD contours for the rounded T-wall.

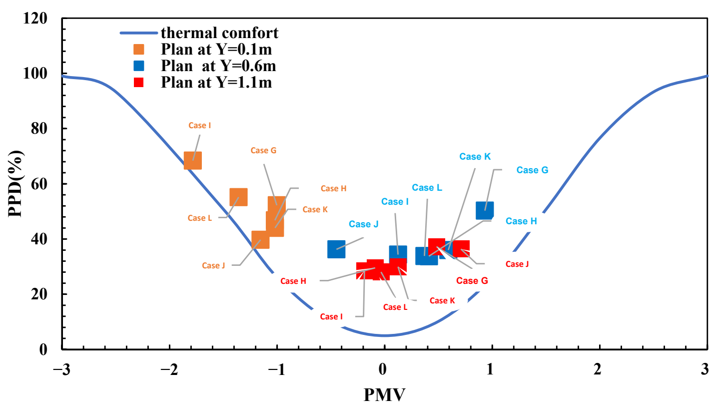

Figure 16. PMV and PPD distributions for six configurations with a rounded T-wall.

3.4. Energy and Exergy Analyses

The energy and exergy efficiency characteristics associated with the building were also explored to determine the impact of various geometric configurations of the T-wall and roof on the room. Simulations in steady state were run for solar radiation intensities of 300, 700, and 1000 W/m^2 to examine the energy and exergy analyses of all geometries.

The energy efficiency of the two types of T-wall and roof layouts for various irradiation intensities is shown in Figure 17. All configurations have a gradual rise in energy efficiency when the radiation intensity is increased. Maximum energy efficiency is found to be more than 20% for the flat T-wall and lower than 20% for the rounded T-wall. Among the other combinations, Cases G and F have the highest value, while Cases J and E have the lowest energy efficiencies.

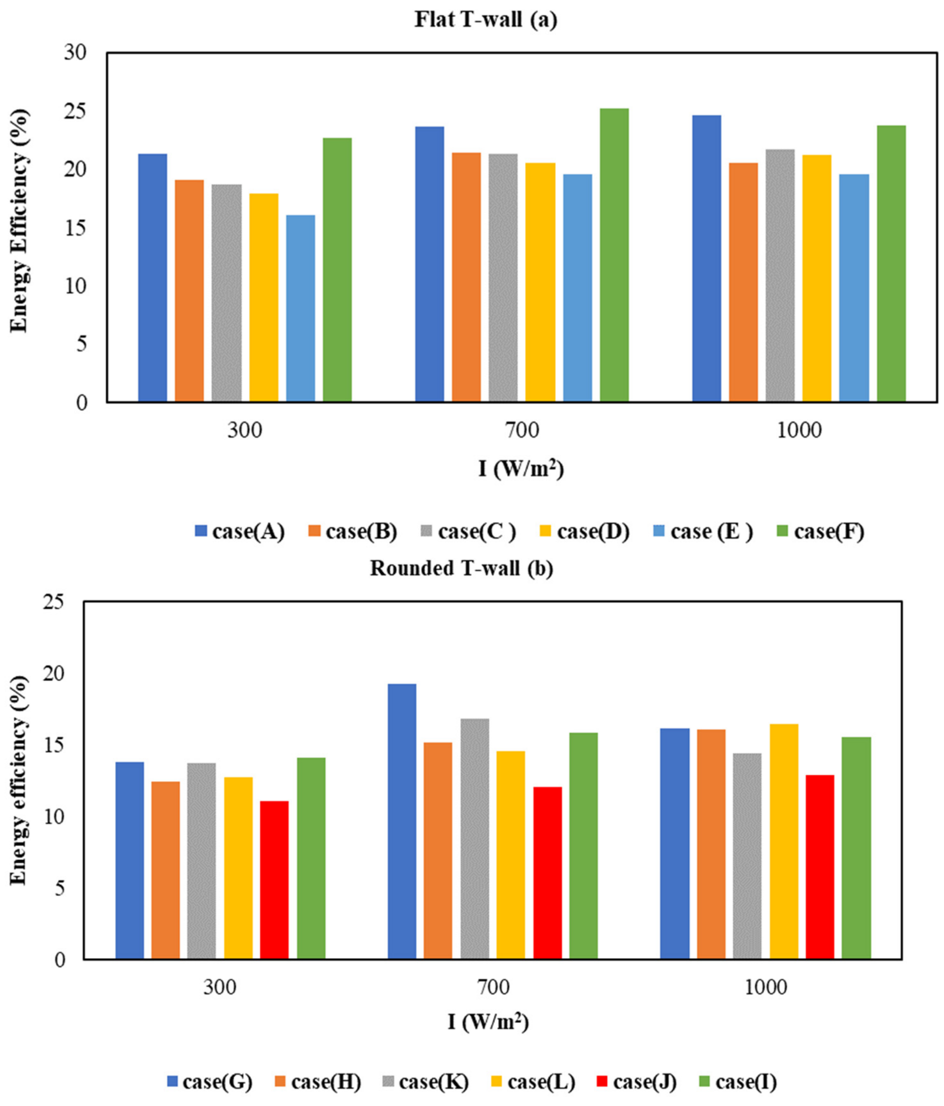

Figure 17. Variation in energy efficiency with solar radiation intensity.

Figure 18 presents the variation in exergy efficiency with the intensity of solar radiation for the two T-walls and roof configurations. It was determined that the increase in the radiation intensity increases the exergy efficiency for all roof configurations. The exergy efficiency ranged between 0.12 W/m^2 (Case J) and 2.44 W/m^2 (Case A) for the flat T-wall. Additionally, Figure 17a offers the exergy efficiency of flat T-wall for three solar radiation intensity values. The exergy efficiency ranged between 0.43 W/m^2 (Case E, I = 300 W/m^2) and 2.44 W/m^2 (Case A, I = 1000 W/m^2) for the flat T-wall. Finally, for the rounded T-wall

(Figure 17b), the exergy efficiency changed between 0.12 W/m^2 (Case J, I = 300 W/m^2) and 1.34 W/m^2 (Case G, I = 700 W/m^2).

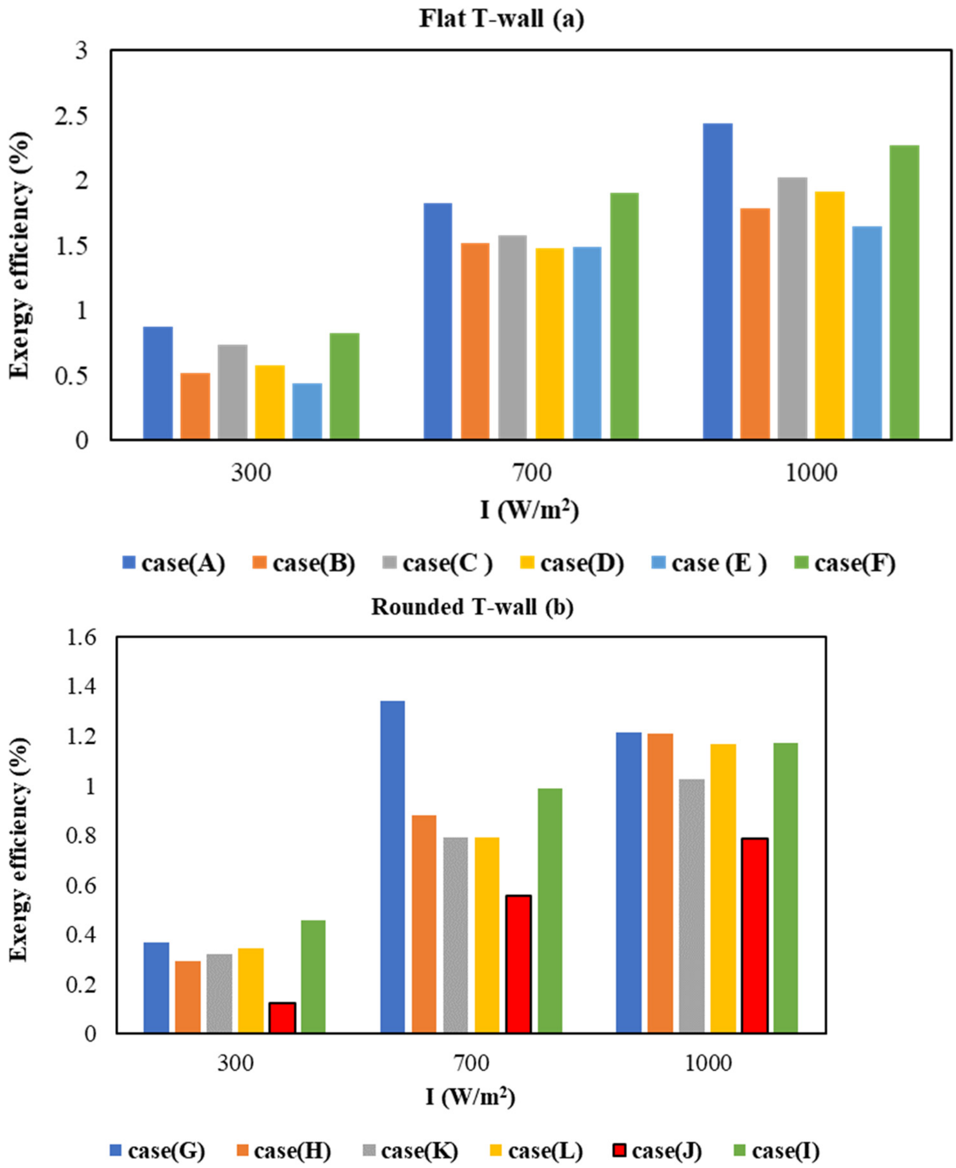

Figure 18. Variation in exergy efficiency with solar radiation intensity.

The energy efficiency of the six different roofs and two different T-wall configurations were relatively high; however, the exergy efficiencies were very low. For the three radiation fluxes, it was observed that the higher energy efficiency was in the case of a flat T-wall (Case F) and was 22% higher than the lowest energy efficiency (Case E). These findings are in line with results from Zhou et al. [51]. On the other hand, for the case of the rounded T-wall, the most efficient situation (Case G) was 27% higher than the least efficient situation (Case J). The maximum difference reached 2% between the rounded T-wall and flat T-wall at I = 700 W/m^2. The flat T-wall was more efficient than the rounded T-wall. This situation was caused by the geometric design of the absorber T-wall, which helped to maintain the duct's homogeneous temperature and boosted energy effectiveness. The findings showed that solar radiation intensity, and especially the T-wall and roof geometries, had a significant impact on energy and exergy efficiency.

4. Conclusions

In this study, a three-dimensional CFD model that is able to adequately exhibit the transparent cover behavior at different radiation wavelengths was developed for the simulation of the two Trombe walls and six roof geometries. The effect of different configurations on the air flow and temperature distributions as well as comfort indexes (PMV and PPD) was evaluated. Moreover, the impacts of geometric configurations and solar radiation intensity on energy and exergy efficiencies were also examined in the study. The investigation made it possible to identify the ideal roof and absorbent T-wall configurations. The main conclusions are as follows:

(a) Flow separation was induced at the corner between the entry and the channel air gap, where the airflow was characterized by severe turbulence close to the floor and roof.
(b) The maximum air velocities in the room reached 0.842 m/s in Case F for the rounded T-wall and 0.989 m/s in Case J for the flat T-wall. This difference was very small. This air velocities were higher than the limit value (0.25 m/s) determined according to ASHRAE Standard 55:2017 [45].
(c) The T-wall successfully lowered the indoor temperature by an average of 6.1 °C. The air temperature differential between the ground and a horizontal plane was held constant in this instance at 0.2 m.
(d) Solar radiation intensity and the T-wall and roof geometries had a significant impact on energy and exergy efficiency. At a solar intensity of 700 W/m^2, Cases G and F had energy efficiencies of 25%, whereas the exergy efficiencies of two T-wall geometries ranged between 1.5 and 2.5%.
(e) At higher solar intensity values, high energy and exergy efficiencies were attained.
(f) The effect of the six different roof geometries on the thermal comfort indices was most profound in the PPD contour distributions in the vicinity of the occupant.
(g) Cases C and L were more comfortable for the standing and sitting activities. The butterfly and shed roofs were best for the two geometries of the T-wall in terms of thermal comfort.
(h) The findings showed that the proposed flat T-wall (2.4 m in height, with a massive wall thickness of 0.30 m, and an air gap of 0.3 m) could provide good thermal performance when integrated with a butterfly roof.
(i) The findings observed in the study revealed that the T-wall should be investigated for different-sized rooms with different window-to-wall ratios in future works. Furthermore, studies should be carried out to form more efficient designs by evaluating the effects on energy and exergy efficiencies of the geometries to be selected in a way different from the T-wall configurations discussed.

In the future, research in this area could further advance our understanding of T-walls. Some prospects for the development of research include smart building technologies where incorporating smart sensors, controls, and automation systems could optimize the operation of T-walls based on real-time environmental conditions, as well as the integration of the T-wall with building energy systems such as passive cooling techniques, active solar technologies, and energy storage solutions.

Author Contributions: M.D.: Formal analysis, Investigation, Methodology, Validation, Writing—original draft; A.Y.: Investigation, Methodology, Writing—original draft, Writing—review & editing; H.A.: Formal analysis, Investigation, Methodology, Validation, Writing—original draft; D.W.: Investigation, Methodology, Writing—original draft, Writing—review & editing; M.A.: Methodology, Writing—original draft, Writing—review & editing, Supervision; H.S.: Methodology, Writing—original draft, Writing—review & editing, Supervision. All authors have read and agreed to the published version of the manuscript.

Funding: This research received no external funding.

Data Availability Statement: Data available on request due to restrictions (privacy).

Conflicts of Interest: The authors declare no conflict of interest.

Abbreviations

Nomenclature and Abbreviations

$\dot{E}_X$	Exergy of solar radiation (kW)
c_a	Water specific heat (J/kg°C)
CFD	Computational fluid dynamics
DC	Direct current
f_{cl}	Clothing area factor
I_{cl}	Clothing insulation (clo or m^2K/W)
M	Metabolic rate (met or W/m^2)
Pa	Partial water vapor pressure (Pa)
PCM	Phase change material
PMW	Predict mean vote
PPD	Predicted percentage of dissatisfied (%)
PV	Photovoltaic
Ra	Rayleigh number
RE	Relative error (%)
T	Temperature (°C)
t	Time (s)
t_{cl}	Surface temperature of clothing (°C)
t_r	Mean radiant temperature (°C)
T-wall	Trombe wall
V	Volume (m^3)
v_{ar}	Relative air speed (m/s)
W	Effective mechanical power (W/m^2)
w	Wind speed (m/s)
Subscripts	
a	Ambient air
b	Buoyancy
c	Convection
d	Destroyed
f	Fluid
i,j	Cartesian coordinates index
in	Inlet
out	Outlet
s	Sun
t	Turbulent
Greek symbols	
λ	Thermal conductivity (W/mK)
μ	Dynamic viscosity (kg/ms)
A_p	Area of the absorber wall, (m^2)
g	Gravitational acceleration (m/s^2)
L	Characteristic length (m)
u	Velocity in the x-direction (m/s)
α	Thermal diffusivity (m^2/s)
ε	Dissipation rate
η	Thermal efficiency (%)
ν	Kinematic viscosity (m^2/s)
ρ	Density (kg/m^3)
σ	Stefan–Boltzman constant (W/m^2K^4)
δ_{ij}	Cartesian coordinates index

References

1. Hampo, C.C.; Ojo, D.O.; Olatunde, D.E.; Isioma, O.J.; Oni, O.O.; Echendu, A.J.; Mathew, M.; Adediji, M.A.; Oladipo, S.F.; Aro, P.O. Life Cycle Assessment of Renewable Energy Technologies in Northern Africa: A Critical Review. Energy Sources, Part A Recover. *Util. Environ. Eff.* **2022**, *44*, 10248–10269. [CrossRef]
2. Li, N.; Fan, M.; Gu, T.; Li, Y.; Yu, B.; Ji, J. The Experimental and Theoretical Analysis on a Trombe Wall with Photo-Thermal Composite Catalytic Purification Blinds. *Build. Environ.* **2023**, *238*, 110379. [CrossRef]

3. Zhang, L.; Cheng, J.; Liu, F.; Li, H.; Dong, Z.; Zhang, X.; Wang, K.; Tian, L.; Liu, H.; Wan, J.; et al. Interaction Effect of Room Size and Opening on Trombe Wall Performance in Sichuan–Tibet Alpine Valley Areas. *Appl. Sci.* **2022**, *12*, 5260. [CrossRef]
4. Wang, D.; Hu, L.; Du, H.; Liu, Y.; Huang, J.; Xu, Y.; Liu, J. Classification, Experimental Assessment, Modeling Methods and Evaluation Metrics of Trombe Walls. *Renew. Sustain. Energy Rev.* **2020**, *124*, 109772. [CrossRef]
5. Mokni, A.; Lashin, A.; Ammar, M.; Mhiri, H. Thermal Analysis of a Trombe Wall in Various Climatic Conditions: An Experimental Study. *Sol. Energy* **2022**, *243*, 247–263. [CrossRef]
6. Sanchez, P.F.; Hancco, L.M. Trombe Walls with Porous Medium Insertion and Their Influence on Thermal Comfort in Flats in Cusco, Peru. *Energy Built Environ.* **2022**, *5*, 194–210. [CrossRef]
7. Siddique, M.; Shahzad, N.; Umar, S.; Waqas, A.; Shakir, S.; Janjua, K.A. Performance Assessment of Trombe Wall and South Façade as Applications of Building Integrated Photovoltaic Systems. *Sustain. Energy Technol. Assess.* **2023**, *57*, 103141. [CrossRef]
8. Prozuments, A.; Borodinecs, A.; Bebre, G.; Bajare, D. A Review on Trombe Wall Technology Feasibility and Applications. *Sustainability* **2023**, *15*, 3914. [CrossRef]
9. Gao, R.; He, W.; Liu, X.; Hu, Z.; Yu, H.; Wang, K. The Performance Analysis of a Novel Photocatalytic-Thermal-Catalytic-Photovoltaic-Trombe Wall System Integrated with Compound Parabolic Concentrator. *Build. Environ.* **2022**, *221*, 109301. [CrossRef]
10. Wang, L.; Zhou, J.; Zhong, W.; Ji, Y.; Yuan, Y. Analysis of Factors Affecting the Performance of a Novel Micro-Channel Heat Pipe PV-Trombe Wall System for Space Heating. *Sustain. Energy Technol. Assess.* **2023**, *58*, 103347. [CrossRef]
11. Guo, S.R.; Jiang, X.C.; Jia, Y.H.; Xiang, M.L.; Liao, Y.X.; Zhang, W.T.; Huang, R.Y.; Long, E.S. Experimental and Numerical Study on Indoor Thermal Environment of Solar Trombe Walls with Different Air-Channel Thicknesses in Plateau. *Int. J. Therm. Sci.* **2023**, *193*, 108469. [CrossRef]
12. Askari, M.; Jahangir, M.H. Evaluation of Thermal Performance and Energy Efficiency of a Trombe Wall Improved with Dual Phase Change Materials. *Energy* **2023**, *284*, 128587. [CrossRef]
13. Baïri, A.; Martín-Garín, A.; Adeyeye, K.; She, K.; Millán-García, J.A. Enhancement of Natural Convection for Improvement of Trombe Wall Performance. An Experimental Study. *Energy Build.* **2020**, *211*, 109788. [CrossRef]
14. Ma, Q.; Wang, X.; Chen, X.; Fukuda, H.; Gao, W.; Wei, X. An Experimental and Numerical Analysis of the Thermal Performance of Double-Layer Trombe Walls. *Energy Sources Part A Recover. Util. Environ. Eff.* **2021**, 1–16. [CrossRef]
15. Zhang, L.; Hou, Y.; Liu, Z.; Du, J.; Xu, L.; Zhang, G.; Shi, L. Trombe Wall for a Residential Building in Sichuan-Tibet Alpine Valley–A Case Study. *Renew. Energy* **2020**, *156*, 31–46. [CrossRef]
16. Wu, S.Y.; Xu, L.; Xiao, L. Air Purification and Thermal Performance of Photocatalytic-Trombe Wall Based on Multiple Physical Fields Coupling. *Renew. Energy* **2020**, *148*, 338–348. [CrossRef]
17. Hu, Z.; Zhang, S.; Hou, J.; He, W.; Liu, X.; Yu, C.; Zhu, J. An Experimental and Numerical Analysis of a Novel Water Blind-Trombe Wall System. *Energy Convers. Manag.* **2020**, *205*, 112380. [CrossRef]
18. Duan, S.; Jing, C.; Zhao, Z. Energy and Exergy Analysis of Different Trombe Walls. *Energy Build.* **2016**, *126*, 517–523. [CrossRef]
19. Zhu, Y.; Zhang, T.; Ma, Q.; Fukuda, H. Thermal Performance and Optimizing of Composite Trombe Wall with Temperature-Controlled DC Fan in Winter. *Sustainability* **2022**, *14*, 3080. [CrossRef]
20. Singh, H.; O'Brien, P.G. Semi-Transparent Water-Based Trombe Walls for Passive Air and Water Heating. *Buildings* **2022**, *12*, 1632. [CrossRef]
21. Bajc, T.; Todorović, M.N.; Svorcan, J. CFD Analyses for Passive House with Trombe Wall and Impact to Energy Demand. *Energy Build.* **2015**, *98*, 39–44. [CrossRef]
22. Bulmez, A.; Brezeanu, A.; Dragomir, G.; Fratu, M.; Iordan, N.; Bolocan, S.; Rozorea, L.; Popa, E.; Năstase, G. CFD Analysis for a New Trombe Wall Concept. *Buildings* **2024**, *14*, 579. [CrossRef]
23. Zhou, S.; Razaqpur, A.G. CFD Modeling and Experimental Validation of the Thermal Performance of a Novel Dynamic PCM Trombe Wall: Comparison with the Companion Static Wall with and without PCM. *Appl. Energy* **2024**, *353*, 121985. [CrossRef]
24. Fidaros, D.; Baxevanou, C.; Markousi, M.; Tsangrassoulis, A. Assessment of Various Trombe Wall Geometries with CFD Study. *Sustainability* **2022**, *14*, 4877. [CrossRef]
25. Corasaniti, S.; Manni, L.; Russo, F.; Gori, F. Numerical Simulation of Modified Trombe-Michel Walls with Exergy and Energy Analysis. *Int. Commun. Heat Mass Transf.* **2017**, *88*, 269–276. [CrossRef]
26. Wu, S.Y.; Zheng, H.; Xiao, L.; Xiang, Y. Experimental Investigation on the Impact of Fin Structure Factors on the Finned-Trombe Wall Thermal Performance. *J. Build. Eng.* **2023**, *70*, 106402. [CrossRef]
27. Al-Sanea, S.A. Thermal Performance of Building Roof Elements. *Build. Environ.* **2002**, *37*, 665–675. [CrossRef]
28. D'Orazio, M.; Di Perna, C.; Di Giuseppe, E. The Effects of Roof Covering on the Thermal Performance of Highly Insulated Roofs in Mediterranean Climates. *Energy Build.* **2010**, *42*, 1619–1627. [CrossRef]
29. Jaffal, I.; Ouldboukhitine, S.E.; Belarbi, R. A Comprehensive Study of the Impact of Green Roofs on Building Energy Performance. *Renew. Energy* **2012**, *43*, 157–164. [CrossRef]
30. Vaishnani, Y.; Ali, S.F.; Joshi, A.; Rakshit, D.; Wang, F. Thermal Performance Analysis of a Naturally Ventilated System Using PMV Models for Different Roof Inclinations in Composite Climatic Conditions. *J. Braz. Soc. Mech. Sci. Eng.* **2020**, *42*, 124. [CrossRef]
31. Moustafa, W.S.; Hegazy, I.R.; Eldabousy, M.M. Roof Geometry as a Factor of Thermal Behavior: Simulation Based Study of Using Vaults and Domes in the Middle East Zone. *Int. J. Low-Carbon Technol.* **2018**, *13*, 204–211. [CrossRef]

32. Sady, H.; Rashidi, S.; Rafee, R. Application of Different Trombe Wall Solutions on the Reduction of Energy Load and Sustainable Development in an Eco-Resort Residential Building in Binalood Region with a Cold and Dry Climate. *Environ. Sci. Pollut. Res.* **2023**, *30*, 68417–68434. [CrossRef] [PubMed]
33. Huberman, N.; Pearlmutter, D.; Gal, E.; Meir, I.A. Optimizing Structural Roof Form for Life-Cycle Energy Efficiency. *Energy Build.* **2015**, *104*, 336–349. [CrossRef]
34. Sornek, K.; Papis-Frączek, K.; Calise, F.; Cappiello, F.L.; Vicidomini, M. A Review of Experimental and Numerical Analyses of Solar Thermal Walls. *Energies* **2023**, *16*, 3102. [CrossRef]
35. Shi, J.; Zhao, C.; Liu, Y. CFD Analysis of Building Cross-Ventilation with Different Angled Gable Roofs and Opening Locations. *Buildings* **2023**, *13*, 2716. [CrossRef]
36. Dhahri, M.; Khalilpoor, N.; Aouinet, H.; Issakhov, A.; Sammouda, H.; Emani, S. Numerical Study on the Thermal Performance of Trombe Wall for Passive Solar Building in Semiarid Climate. *Int. J. Photoenergy* **2021**, *2021*, 6630140. [CrossRef]
37. Dhahri, M.; Nekoonam, S.; Hana, A.; El Haj Assad, M.; Arıcı, M.; Sharifpur, M.; Sammouda, H. Thermal Performance Modeling of Modified Absorber Wall of Solar Chimney-Shaped Channels System for Building Ventilation. *J. Therm. Anal. Calorim.* **2021**, *145*, 1137–1149. [CrossRef]
38. Hassan, A.M. Solar Chimney Performance Driven Air Ventilation Promotion: An Investigation of Various Configuration Parameters. *Buildings* **2023**, *13*, 2796. [CrossRef]
39. Bevilacqua, P.; Bruno, R.; Gallo, S.; Szyszka, J. A Validated Multi-Physic Model for the Optimization of an Innovative Trombe Wall for Winter Use. *J. Build. Eng.* **2024**, *86*, 108915. [CrossRef]
40. Wu, S.Y.; Yan, X.Q.; Xiao, L. Numerical Analysis on Geometric and Shape Parameters of Solar Dual-Catalytic Trombe Wall Performance. *Solar Energy* **2020**, *199*, 460–473. [CrossRef]
41. Hu, Z.; He, W.; Hong, X.; Ji, J.; Shen, Z. Numerical Analysis on the Cooling Performance of a Ventilated Trombe Wall Combined with Venetian Blinds in an Office Building. *Energy Build.* **2016**, *126*, 14–27. [CrossRef]
42. Hernández-López, I.; Xamán, J.; Chávez, Y.; Hernández-Pérez, I.; Alvarado-Juárez, R. Thermal Energy Storage and Losses in a Room-Trombe Wall System Located in Mexico. *Energy* **2016**, *109*, 512–524. [CrossRef]
43. Abdeen, A.; Serageldin, A.A.; Ibrahim, M.G.E.; El-Zafarany, A.; Ookawara, S.; Murata, R. Experimental, Analytical, and Numerical Investigation into the Feasibility of Integrating a Passive Trombe Wall into a Single Room. *Appl. Therm. Eng.* **2019**, *154*, 751–768. [CrossRef]
44. Rabani, M.; Rabani, M. Heating Performance Enhancement of a New Design Trombe Wall Using Rectangular Thermal Fin Arrays: An Experimental Approach. *J. Energy Storage* **2019**, *24*, 100796. [CrossRef]
45. *ANSI/ASHRAE Standard 55-2017*; Thermal Environmental Conditions for Human Occupancy. ASHRAE Inc.: Peachtree Corners, GA, USA, 2017.
46. Fanger, P.O. *Thermal Comfort. Analysis and Applications in Environmental Engineering*; Danish Technical Press: Copenhagen, Denmark, 1970.
47. Al-Rawi, M. The Thermal Comfort Sweet-Spot: A Case Study in a Residential House in Waikato, New Zealand. *Case Stud. Therm. Eng.* **2021**, *28*, 101530. [CrossRef]
48. Fanger, P.O. Assessment of Man's Thermal Comfort in Practice. *Occup. Environ. Med.* **1973**, *30*, 313–324. [CrossRef] [PubMed]
49. Markov, D. Practical Evaluation of the Thermal Comfort Parameters. *Annu. Int. Course Vent. Indoor Clim. Avangard Sofia* **2002**, *70*, 158–170.
50. Irshad, K.; Habib, K.; Thirumalaiswamy, N.; Kareem, M.W. Thermal Comfort Analysis of Building Assisted with Photo Voltaic Trombe Wall. *MATEC Web Conf.* **2016**, *38*, 02003. [CrossRef]
51. Zhou, L.; Huo, J.; Zhou, T.; Jin, S. Investigation on the Thermal Performance of a Composite Trombe Wall under Steady State Condition. *Energy Build.* **2020**, *214*, 109815. [CrossRef]